electronic reprint

Acta Crystallographica Section A
Foundations of Crystallography
ISSN 0108-7673

Electron crystallographic image-processing investigation and superstructure determination for $(Pb_{0.5}Sr_{0.3}Cu_{0.2})Sr_2(Ca_{0.6}Sr_{0.4})Cu_2O_y$

J. Liu, F. H. Li, Z. H. Wan, H. F. Fan, X. J. Wu, T. Tamura and K. Tanabe

Acta Crystallographica Section A
Foundations of Crystallography
ISSN 0108-7673

Received 30 January 2001
Accepted 9 May 2001

Electron crystallographic image-processing investigation and superstructure determination for $(Pb_{0.5}Sr_{0.3}Cu_{0.2})Sr_2(Ca_{0.6}Sr_{0.4})Cu_2O_y$

J. Liu,[a]† F. H. Li,[a]* Z. H. Wan,[a] H. F. Fan,[a] X. J. Wu,[b] T. Tamura[b] and K. Tanabe[b]

[a]Institute of Physics and Center for Condensed Matter Physics, Chinese Academy of Sciences, PO Box 603, Beijing 100080, People's Republic of China, and [b]Superconductivity Research Laboratory, International Superconductivity Technology Center, 10-13 Shinonome, 1-Chome, Kyoto-Ku, Tokyo 135, Japan. Correspondence e-mail: lifh@aphy.iphy.ac.cn

An electron crystallographic image-processing technique based on the combination of high-resolution electron microscopy and electron diffraction has been developed to investigate the commensurate structural modulation in the high-T_c superconductor $(Pb_{0.5}Sr_{0.3}Cu_{0.2})Sr_2(Ca_{0.6}Sr_{0.4})Cu_2O_y$. After symmetry averaging, a structure image was obtained by image deconvolution at the resolution limited by that of the electron microscope. Then phase extension was employed to enhance the image resolution up to about 1.25 Å by means of the electron diffraction data corrected with an empirical method. In the final projected potential map, the occupational and/or positional modulation is clearly observed for all atoms, including oxygen. The key points of determining superstructures by the technique are studied and discussed.

1. Introduction

Since the first Pb-based high-T_c superconductor discovered by Cava *et al.* (1988), many Pb-based cuprates have been synthesized (Rouillon *et al.*, 1989; One & Horiuchi, 1994; Yamauchi *et al.*, 1995). The common feature in compounds of this kind is the structural modulation and the modulation wave is different for different samples (Rouillon *et al.*, 1989; One & Horiuchi, 1994; Wu *et al.*, 1995). The structural modulation originates from a periodic fluctuation of atoms on their occupation and/or position relative to those in the basic structure. If the periodicity of the structural modulation is commensurate with the periodicity of basic structure, the modulated crystal structure is called a commensurate modulated structure or superstructure, otherwise it is called an incommensurate modulated structure (de Wolff, 1974). The commensurate modulated structure remains three-dimensional (3D) periodical and the structure analysis can be carried out in the conventional 3D space.

In X-ray crystallography, it has been proved that direct methods are powerful in solving commensurate (Fan *et al.*, 1983) as well as incommensurate modulated structures (Hao, Liu & Fan, 1987). However, when the crystal size is very small as for the present compound, X-ray crystallographic techniques are difficult to use, while electron crystallography provides alternative choices. One approach is to determine the crystal structure by electron diffraction, which has been shown to be an effective way, especially for textured materials (Vainstein, 1964) and inorganic compounds (Dorset, 1995). The second approach is by high-resolution electron microscopy (HREM) (Buseck *et al.*, 1988), which does not suffer the phase problem that all diffraction methods do. The trial-and-error method is the traditional and most popular method of crystal structure determination in HREM. By this method, the resolution of the resulting image is limited by the resolution of the electron microscope so that not all atoms can be resolved individually with the medium-voltage microscope, even leaving aside the problem of finding the structure image when the examined structure is completely unknown beforehand. The exit-wave reconstruction and image deconvolution are two main alternative methods of crystal structure determination in HREM. In the case of image reconstruction, the phase and amplitude of the exit wave formed at the bottom plane of the sample is recovered from two or more images taken with different defocus values (Schiske, 1968; Misell, 1973; Kirkland, 1984; Kirkland *et al.*, 1985; Saxton, 1986; Van Dyck & Op de Beeck, 1990; Coene *et al.*, 1992; Van Dyck *et al.*, 1996; Coene *et al.*, 1996; Tang *et al.*, 1996; Van Dyck & Op de Beeck, 1996). The reconstructed phase image reflects the projected crystal structure when the sample is very thin. For thicker crystals, the structure can be derived from the exit wave by solving the inverse problem of dynamical electron diffraction. In the case of image deconvolution, the projected crystal structure is obtained from a single image based on the weak-phase-object approximation (WPOA) (Uyeda & Ishizuka, 1974; Unwin & Henderson, 1975; Li & Fan, 1979; Hovmöller *et al.*, 1984; Han *et al.*, 1986; Hu & Li, 1991) or based on the channeling theory (Hu & Tanaka, 1999; Van Dyck & Op de Beeck, 1996). To combine electron diffraction and HREM provides another approach. For instance, the image deconvolution technique

† Present address: Institute of Molecular Biophysics, Florida State University, Tallahassee, FL 32306, USA.

based on the direct method developed in X-ray crystallography (Han *et al.*, 1986) and that based on the principle of maximum entropy (Hu & Li, 1991) have been successfully applied to solid-state compounds (Hu *et al.*, 1992; Fu *et al.*, 1994; Lu *et al.*, 1997; Liu *et al.*, 1998; Jiang *et al.*, 1999) as well as proteins (Yang & Li, 2000). Generally, the resolution of such an obtained deconvoluted image is limited by the resolution of the electron microscope. The image-deconvolution technique was also employed to reveal the crystal defects from the image taken with a field-emission electron microscope and the resolution of the deconvoluted image can reach the information resolution limit of the microscope (He *et al.*, 1997; Wang *et al.*, 2000; Li *et al.*, 2000). After obtaining the structure that is resolution limited by the resolution of the microscope, the phase extension based on the kinematical diffraction is carried out by means of direct methods (Dorset & Hauptman, 1976; Fan *et al.*, 1985) and the maximum-entropy likelihood method (Bricogne & Gilmore, 1990) is carried out to obtain the high-resolution structure. Recently, dynamical direct methods have been developed (Sinkler & Marks, 1999) to attain the high-resolution structure.

The two-stage electron crystallographic image-processing technique (Fan *et al.*, 1991; Li, 1994), which consists of image deconvolution and phase extension, has been successfully applied to determine ordinary 3D periodic structures (Hu *et al.*, 1992; Lu *et al.*, 1997; Jiang *et al.*, 1999) as well as incommensurate modulated structures (Fu *et al.*, 1994; Liu *et al.*, 1998). Recently, the electron crystallographic image-processing technique has been incorporated into the *VEC* package (Wan, Li & Fan, unpublished). This makes the crystal structure analysis more convenient.

In the present paper, the two-stage electron crystallographic image-processing technique combined with the diffraction-intensity correction is applied to determine the commensurate modulated structure in a Pb-based high-T_c superconductor $(Pb_{0.5}Sr_{0.3}Cu_{0.2})Sr_2(Ca_{0.6}Sr_{0.4})Cu_2O_y$ (hereafter called 'Pb'-1212) (Yamauchi *et al.*, 1995). The experimental electron diffraction intensities were corrected by an empirical method reported by Huang, Liu *et al.* (1996) to approximate the square structure factors. No prior structural information about the superstructure was used. The methods of determining superstructures by this technique are also studied and discussed.

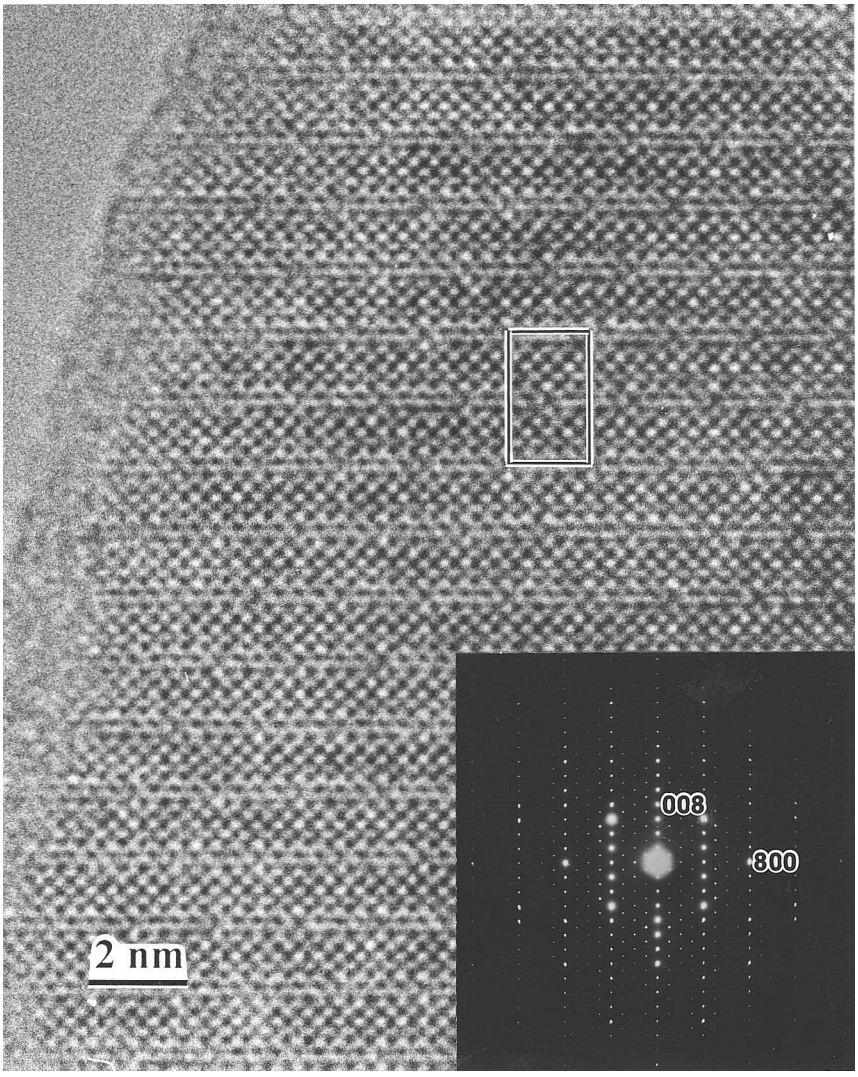

Figure 1
Experimental [010] high-resolution electron-microscope images of 'Pb'-1212 with the corresponding experimental EDP inset. The rectangle indicates the supercell.

2. Experimental

A specimen of 'Pb'-1212 for electron diffraction and HREM observation was prepared by crushing. The fine fractions were transferred onto a copper grid covered with holey carbon film and observed with an H-9000NA electron microscope at an accelerating voltage of 300 kV. A series of [010] electron diffraction patterns (EDPs) were taken with different exposure times from the same area, which was selected to be as thin as possible. The corresponding high-resolution electron-microscope image was obtained by using a JEM-4000EX electron microscope operated under 400 kV. The spherical aberration coefficient of the objective lens is 1.0 mm, the standard deviation of Gaussian distribution of defocus due to the chromatic aberration (hereafter called chromatic aberration defocus spread) about 100 Å and the resolution 1.7 Å.

The negatives of the EDPs were scanned using a Perkin–Elmer PDS microdensitometer with a raster size of 30×30 µm. The program *PLANE* (Cheng *et al.*, 1994) was used for calculating the density–intensity characteristic curve of the film and measuring the integral diffraction

intensity for all diffraction peaks. Intensities of symmetry-related reflections were averaged. The high-resolution electron micrograph was digitized by using a CCD camera.

The basic structure of 'Pb'-1212 belongs to the orthorhombic system with lattice parameters $a_o = 3.81$, $b_o = 3.83$ and $c_o = 12.13$ Å. It is isomorphic to the crystal structure of the high-temperature superconducting compound $TlBa_2CaCu_2O_y$ (Wu *et al.*, 1995). The unit cell of the superstructure (hereafter called supercell) equals $4a_o \times b_o \times 2c_o$ and the space group is *Bmmm*. Fig. 1 shows the experimental high-resolution image of 'Pb'-1212 projected along the [010] direction together with the corresponding EDP inset. The rectangle indicates the supercell. The noise filtering and symmetry averaging were performed for a thin area from Fig. 1 to obtained symmetry-average images. The averaging according to the basic cell (unit cell of basic structure) yields the symmetry-average image of the basic structure (Fig. 2*a*), while the averaging according to the supercell yields the symmetry-average image of the superstructure (Fig. 2*b*). Then the image deconvolution was carried out for the two symmetry-average images. The spherical aberration coefficient and the chromatic aberration defocus spread were 1.0 mm and 100 Å, respectively, and the astigmatism was ignored. Thus the crux of image deconvolution is in determining the defocus value of the original image. In the present case, the defocus value was searched (Han *et al.*, 1986) for the symmetry-average image of basic structure from 17 independent basic reflections by use of the program *VEC* based on the principle of direct methods (Fu & Fan, 1994). Trial defocus values were assigned according to the practical imaging condition from −900 to 0 Å with an interval of 10 Å. The corresponding combined figure of merit (CFOM) which serves as a criterion in direct methods (Debaerdemaeker *et al.*, 1985; Woolfson & Fan, 1995) was calculated. The curve given in Fig. 3 shows the CFOM changing with the change of trial defocus value. Generally, the greater the value of CFOM, the more reasonable the set of trial structure factors. It can be seen that there are two highest peaks in the curve of CFOM in Fig. 3 marked *a* and *b* with the corresponding defocus values −780 and −430 Å, respectively. The deconvoluted images obtained from Fig. 2(*a*) with these two defocus values are given in Figs. 4(*a*) and (*b*), respectively. To select the true solution between the two, the number of black dots in the unit cell, and the size and arrangement of the black dots are analyzed. In the structure image, all atoms must appear black. From the view of crystallographic chemistry, it is reasonable to consider that the deconvoluted image shown in Fig. 4(*a*) reflects the true

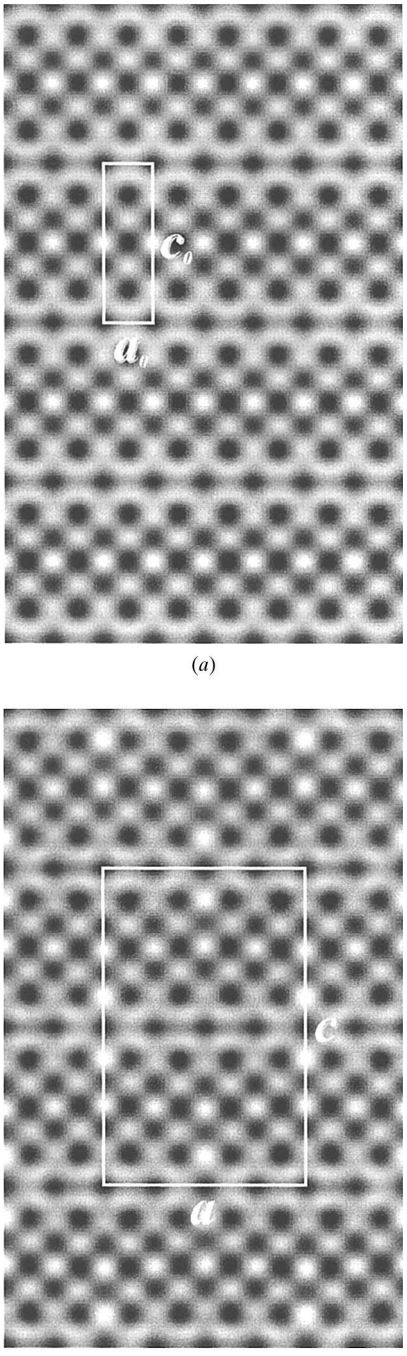

Figure 2
Symmetry-average images for (*a*) the basic structure and (*b*) the superstructure of 'Pb'-1212.

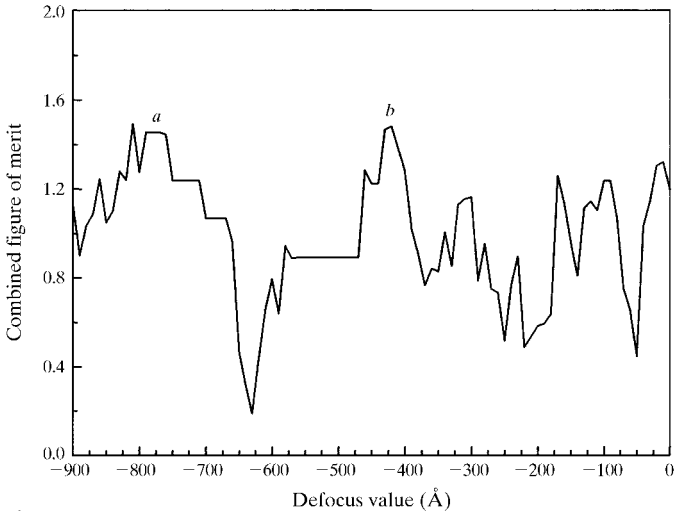

Figure 3
Curve showing the change of combined figure of merit (CFOM) with the defocus.

structure rather than Fig. 4(*b*) because the distances between the small black dots in Fig. 4(*b*) are not consistent with those of metallic atoms. However, in this image the arrangement of the white dots in Fig. 4(*b*) is similar to that of the black dots in Fig. 4(*a*). This means that Fig. 4(*b*) is almost the reverse of Fig. 4(*b*) in contrast. Such a phenomenon is common in image deconvolution, especially for simple crystal structures with a small unit cell as discussed by Huang, He & Li (1996) regarding the multisolution of image deconvolution based on the principle of maximum entropy (Hu & Li, 1991). Therefore, the determined defocus value of the experimental image is −430 Å and the deconvoluted image (Fig. 4*a*) reflects the projected basic structure, where all metallic atoms are resolved as individual black dots. Because the image resolution is limited by the resolution of the electron microscope, oxygen atoms are not visible. Hence the projected structure revealed in the deconvoluted image is a low-resolution structure.

The image deconvolution was performed to the average image of the superstructure (Fig. 2*b*) with the same defocus value (−430 Å) and the result is shown in Fig. 4(*c*). All metallic atoms are also clearly resolved. The structural modulation in the deconvoluted image (Fig. 4*c*) is clearly seen by comparison with Fig. 4(*a*). Although the resolution of the deconvoluted images (Figs. 4*a* and *c*) is too low to resolve the oxygen atoms, these images provide a good basis for the subsequent correction of experimental electron diffraction data and phase extension.

3. High-resolution structure

3.1. Electron diffraction intensity correction

The high-resolution projected structure can be obtained by phase extension based on the phases of structure factors obtained from the deconvoluted image and the amplitudes of structure factors obtained from the electron diffraction data. It was reported that the electron diffraction intensities usually deviate from the square structure factors and an empirical method was proposed for correcting the electron diffraction data (Huang, Liu *et al.*, 1996). The essence of the method is to propose a partial structure model containing atoms seen in the deconvoluted image, and then the correction is based on the partial structure factors calculated for the proposed model. Obviously, the partial structure factors are kinematical rather than dynamical. In the present case, based on Fig. 4(*a*), a two-dimensional model of the basic structure containing only metallic atoms was proposed. The partial structure factors were calculated accordingly. Scaling factors are calculated for all systematically strong reflections (reflections of the basic

Table 1
Independent reflections of basic structure.

Index				
h	*k*	*l*	Amplitude	Phase (°)
0	0	1	19.34	180
0	0	2	16.77	0
0	0	3	20.5	0
1	0	0	16.95	180
1	0	1	21.58	0
1	0	2	16.55	0
0	0	4	24.18	0
1	0	3	35.5	0
0	0	5	23.58	0
1	0	4	20.68	180
1	0	5	10.79	0
0	0	6	18.81	0
2	0	0	31.74	0
2	0	1	12.65	0
2	0	2	8.65	0
1	0	6	11.1	0
0	0	7	22.26	180

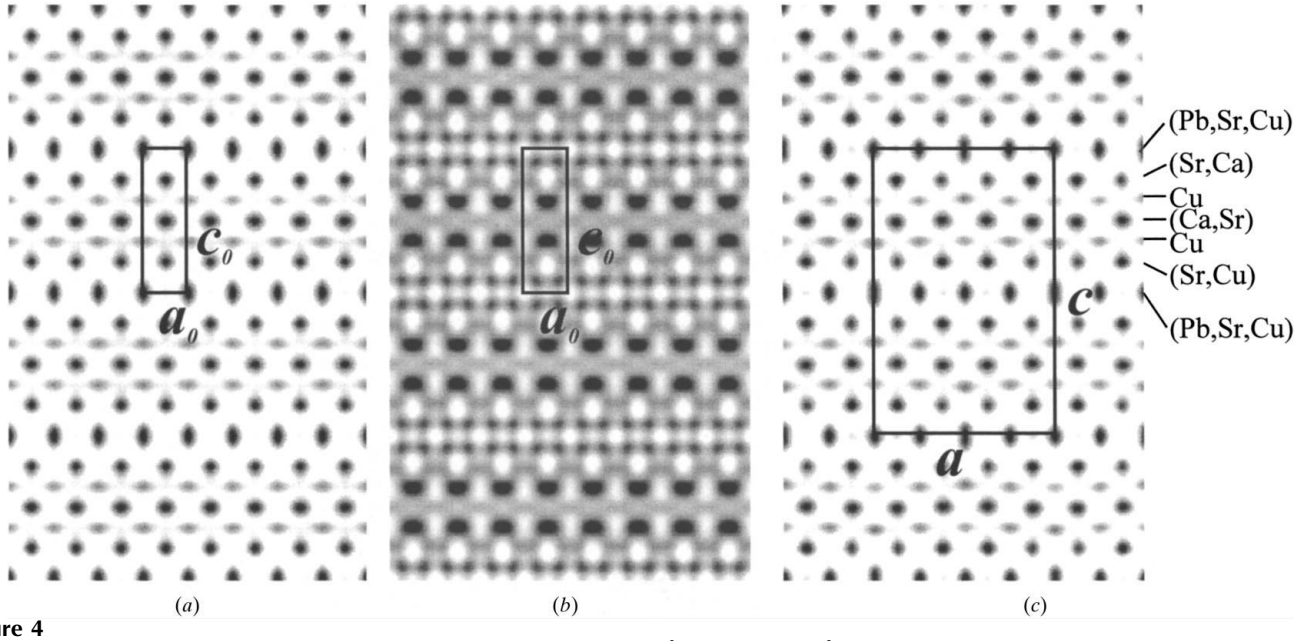

Figure 4
Deconvoluted images obtained from Fig. 2(*a*) with defocus value (*a*) −430 Å and (*b*) −780 Å; (*c*) deconvoluted image obtained from Fig. 2(*b*) with defocus value −430 Å.

Table 2
Independent reflections of superstructure structure.

Index					Index				
h	*l*	Amplitude	Corrected amplitude	Phase (°)	*h*	*l*	Amplitude	Corrected amplitude	Phase (°)
1	1	11.15	7.59	0	0	2	19.34	13.15	180
2	0	7.61	5.18	180	1	3	3.47	2.36	180
2	2	4.86	3.31	180	0	4	16.77	11.4	0
3	1	4.79	3.26	180	2	4	3.74	2.54	0
1	5	4.61	3.13	180	3	3	3.52	2.39	0
0	6	20.5	13.94	0	4	0	16.95	11.53	180
4	2	21.58	20.77	0	2	6	5.35	5.32	180
3	5	4.05	4.02	0	1	7	5.74	5.71	0
4	4	16.55	16.44	0	0	8	24.18	25.16	0
5	1	6.03	6.4	180	3	7	4.84	5.13	180
5	3	8.27	8.77	0	2	8	5.74	6.08	0
4	6	35.5	37.63	0	1	9	8.57	9.48	0
5	5	11.31	12.52	0	6	0	4.73	5.23	180
6	2	3.31	3.66	180	0	10	23.58	26.09	0
3	9	3.63	4.11	0	4	8	20.68	23.39	180
6	4	4.63	5.22	180	2	10	6.06	6.82	180
5	7	5.89	6.64	180	1	11	7.07	7.97	0
7	1	3.67	4.13	0	6	6	3.38	3.81	180
7	3	2.43	2.73	0	4	10	10.79	12.16	0
3	11	4.77	4.91	0	0	12	18.81	19.35	0
5	9	3.85	4.07	180	7	5	2.83	2.99	180
2	12	4.43	4.68	180	6	8	1.91	2.02	180
8	0	31.74	33.53	0	8	2	12.65	13.22	0
1	13	4.6	4.86	180	7	7	2.28	2.41	0
8	4	8.65	9.13	0	5	11	3.89	4.03	0
4	12	11.1	11.5	0	6	10	2.67	2.29	180
3	13	4.37	3.74	0	0	14	22.26	19.07	180
8	6	7.6	7.41	0	7	9	4.09	4.22	0
9	1	3.66	3.78	0	2	14	1.87	1.93	180
9	3	3.51	3.63	180	8	8	16.54	17.08	0
1	15	3.69	3.68	0	9	5	2.75	2.75	180
5	13	3.97	3.96	0	6	12	2.13	2.12	180
4	14	11.98	11.95	0	7	11	2.75	3.05	0
3	15	3.51	3.91	0	10	0	3.29	3.65	180
9	7	2.97	3.31	0	0	16	11.11	12.35	0
10	2	2.79	3.25	180	8	10	11.53	13.45	0
2	16	1.62	1.95	180	10	4	2.48	3	180
9	9	3.84	4.65	0	6	14	1.63	1.97	180
5	15	4.65	5.63	0	10	6	1.87	2.26	180
1	17	3.52	4.26	0	7	13	2.4	2.9	180
4	16	11.32	13.7	180	8	12	7.17	8.41	0
11	1	2.25	2.45	180	3	17	1.6	1.75	180
11	3	1.88	2.05	0	10	8	1.44	1.57	180
0	18	9.94	10.84	0	9	11	3.6	3.66	0
11	5	2.2	2.24	0	2	18	1.83	1.86	180
6	16	1.54	1.57	180	7	15	2.51	2.55	0
5	17	2.49	2.53	180	10	10	1.36	1.38	180
11	7	1.98	2.01	0	8	14	15.57	15.82	180
12	0	5.56	6.07	0	1	19	2.21	2.49	0
4	18	6.76	7.63	0	12	2	6.91	7.46	0
9	13	3.41	4.16	180					

structure). Observed diffraction intensities of the strong reflections were corrected as given by Lu *et al.* (1997) by using the method of Huang, Liu *et al.* (1996). Systematically weak reflections (reflections for the superstructure) were corrected with the same scaling factor as that for the nearest strong reflection.

3.2. Phase extension

To obtain high-resolution structure information for 'Pb'-1212, the direct-method phase extension was used to enhance the resolution. In X-ray crystallography, two ways are available to extend phases of reflections for superstructures. One is to derive the phases of all reflections simultaneously (including systematically strong and weak reflections). The other is in two steps (Fan *et al.*, 1983). The first step is to derive phases of systematically strong reflections as usual. In the second step, phases derived in the first step are treated as known phases to derive the phases of the systematically weak reflections. The latter procedure has been proved much more efficient in X-ray crystallography (Fan *et al.*, 1983, 1988). However, it is still interesting to see whether the procedure of deriving phases of all reflections, strong and weak, simultaneously is feasible in electron crystallography.

Starting phases of structure factors for the phase extension were obtained from the Fourier transform of the deconvoluted image of the superstructure shown in Fig. 4(*a*) and amplitudes from the corrected diffraction data as mentioned above (Table 1). Phases of high-scattering-angle reflections (including systematically strong and systematically weak reflections, as shown in Table 2) were derived by means of the program *VEC*. The resultant projected potential map (PPM) of resolution close to 1.25 Å is shown in Fig. 5(*a*). By comparison to Fig. 4(*c*), the occupational and positional modulations are seen clearly in Fig. 5(*a*). Some additional weak dots representing the oxygen atoms also appear.

Fourier synthesis was employed to refine the PPM. For this the structure factors are calculated for the structure model corresponding to the PPM given in Fig. 5(*a*). Then a new PPM was calculated with phases identical to the calculated structure factors and amplitudes unchanged. Fig. 5(*b*) shows the final PPM of the superstructure with 1.25 Å resolution after two cycles of Fourier synthesis. All unoverlapped atoms including oxygen are clearly resolved in this map. Moreover, the structural modulation is more dominant than in Fig. 5(*a*). Because the derived PPMs are closely related to the kinematical partial structure factor, it is reasonable to assume that the blackness of dots is monotonous with the atomic weight. Fig. 5(*b*) shows that in 'Pb'–O layers for every four neighbor metallic atoms there are one strongest black dot, which should represent the Pb atom, one weakest black dot, which should represent the Cu atom, and another two black dots represent both the Pb and the Sr atoms partly. In the 'Sr'–O layer, the contrast change for metallic atoms indicates a partial substitution of Ca atoms for Sr atoms. The other prominent feature is the strong occupational modulation of oxygen in the 'Sr'–O layer, namely (Sr,Ca)–O layer, while the occupational modulation in the Cu–O layer is relatively weak. Besides, there exists positional modulation in 'Ca'–O, namely (Ca,Sr)–O and Cu–O layers. Obviously, this is related to the substitution of Sr and Cu for Pb in the 'Pb'–O layer. The [010] projection of the schematic superstructure model derived from the final PPM for 'Pb'-1212 is shown in Fig. 6(*a*). Table 3 shows the atomic parameters determined from Fig. 5(*b*). Although what is determined is the [010] projected structure, the three-dimensional structure is obtained straightforwardly because the basic structure is known in advance (Wu *et al.*, 1995) and the structural modulation occurs merely in the [100] and [001] directions.

A series of images was calculated for the obtained superstructure model with different crystal thicknesses and defocus value −430 Å, which was determined as mentioned above. The image with thickness 38.3 Å is shown in Fig. 6(*b*). Its contrast is in agreement with the average experimental image (Fig. 2*b*). Fig. 6(*c*) is the image simulated with the same parameters as Fig. 6(*b*) but all oxygen atoms are ignored. It is seen that the contrast of Fig. 6(*c*) is different from Fig. 6(*b*). The former has a background brighter than the latter. This means that, although oxygen atoms appear neither in Fig. 6(*b*) nor in Fig. 2(*b*), they do contribute to the image contrast, and confirms the determined structure including the positions of the oxygen atoms.

4. Discussion and conclusions

The electron crystallographic image-processing technique has been studied and applied to commensurate modulated structure determination. The superstructure of 'Pb'-1212 has been

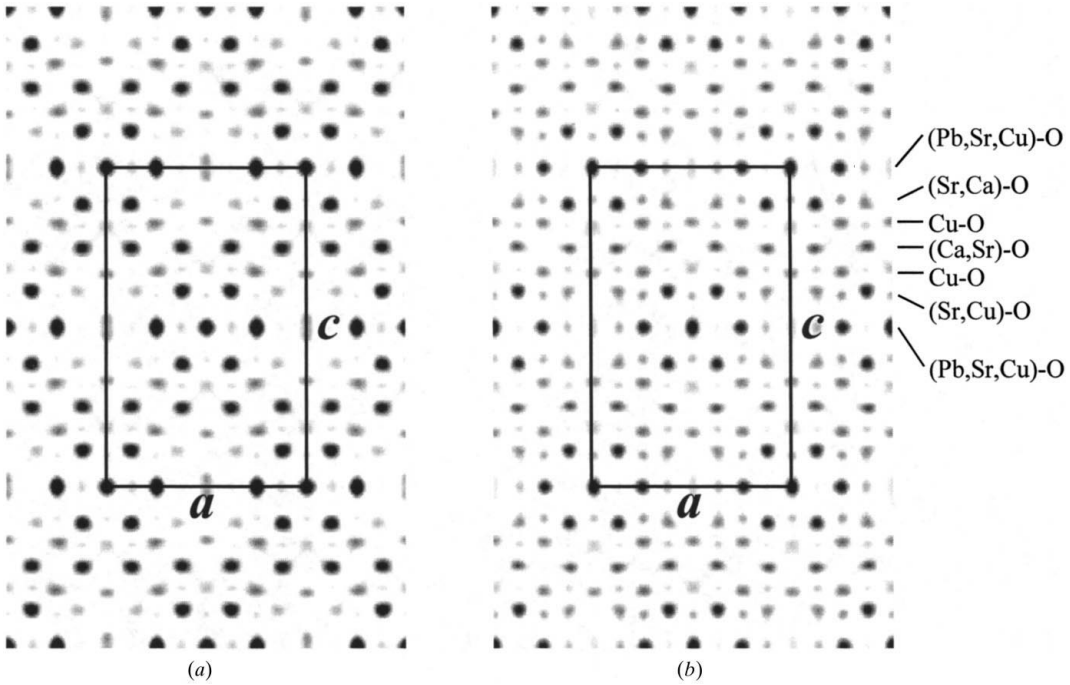

Figure 5
Projected potential maps of 'Pb'-1212 obtained (*a*) after phase extension and (*b*) after two cycles of Fourier synthesis from (*a*).

Table 3
Positional parameters of 'Pb'-1212 in [010] projection.

Symmetry in [010] projection $\frac{3}{4}$ *B*2*mm*

Atom	Site	*x*	*z*
Pb	2(*a*)	0.000	0.000
Pb(Sr)	4(*d*)	0.250	0.000
Cu(1)	2(*b*)	0.500	0.000
Sr(1)	8(*f*)	0.125	0.113
Sr(Ca)	8(*f*)	0.374	0.109
Cu(2)	8(*f*)	0.250	0.184
Cu(3)	4(*e*)	0.000	0.174
Cu(4)	4(*e*)	0.500	0.170
Ca(Sr)	8(*f*)	0.125	0.253
O(1)	4(*d*)	0.125	0.000
O(2)	4(*d*)	0.375	0.000
O(3)	4(*e*)	0.000	0.105
O(4)	8(*f*)	0.250	0.101
O(5)	8(*f*)	0.122	0.179
O(6)	8(*f*)	0.376	0.183

analyzed using the two-stage electron crystallographic image-processing technique. All atoms including oxygen are resolved in the final PPM and the structural modulation, including both the occupational and/or positional modulation, can been seen directly and clearly.

Two approaches of the direct-methods phase extension have been applied to obtain the high-resolution modulated information. They both work in this particular case if the modulated information from the deconvoluted image is included. Generally, both of these approaches could be considered for superstructure determination. For a strongly modulated superstructure, the one-step approach of phase extension would be better; while for a weakly modulated superstructure a two-step approach may be favorable.

Usually, a high-resolution electron-microscope image taken from a thin sample is reliable enough for obtaining the low-resolution structure by image deconvolution. For deriving the high-resolution structure by phase extension, high-quality diffraction data are essential. The empirical method for electron diffraction correction (Huang, Liu *et al.*, 1996) provides a practical way to overcome the difficulty in using the electron diffraction data for structure analysis.

The essentials for commensurately modulated structure determination by the present technique are summarized in the following. Firstly, for convenience, the defocus value can be determined from the average image according to the unit cell of the basic structure. Secondly, by using the determined defocus value, the image deconvolution is performed on the symmetry-average image of the superstructure to obtain the deconvoluted image. Thirdly, the phase extension is carried out in combination with the diffraction data correction. At first, the scaling factors for correcting diffraction data are calculated only for the main reflections (systematically strong reflections) of a superstructure. Then each scaling factor is applied to the main reflection as well as the nearby satellites (systematically weak reflections). In this stage, the phases of main reflections as well as satellites are derived at the same time.

The present work indicates that the two-stage image-processing technique combined with the empirical method of electron diffraction intensity correction is an efficient approach for solving commensurately modulated structures even for crystals containing very heavy atoms such as Pb and Sr. This provides a powerful tool that can be extended to crystal structure determination of other important solid-state materials.

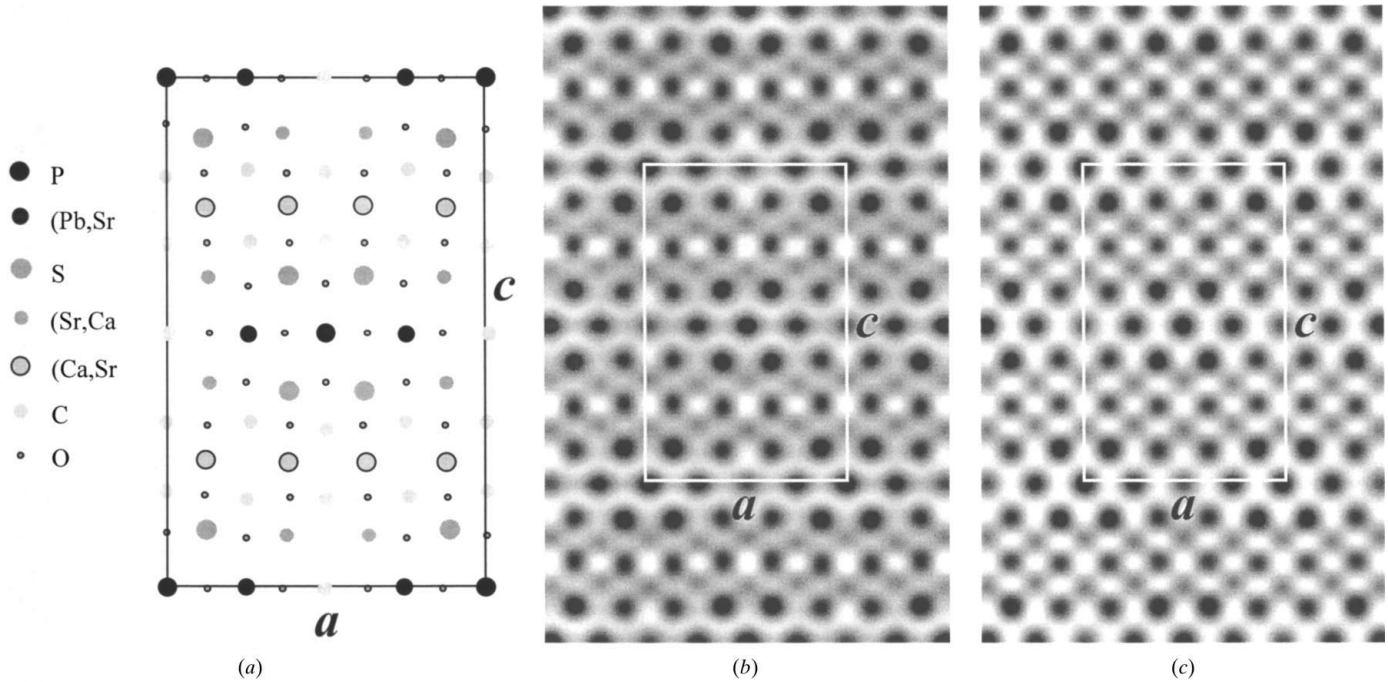

Figure 6
(*a*) A schematic superstructure model of 'Pb'-1212, (*b*) simulated image of 'Pb'-1212 with defocus value −430 Å and thickness 38.3 Å, and (*c*) simulated image with the same parameters but all oxygen atoms are ignored.

JL, FHL, ZHW and HFF are indebted to Drs J. Y. Xing and B. Lu for scanning the negatives of EDPs. This work is supported by the Ministry of Sciences and Technology of China (NKBRSF-G1999064603), the National Natural Science Foundation of China and the New Energy and Industrial Technology Development Organization for the R & D of Industrial Science and Technology Frontier Program of Japan.

References

Bricogne, G. & Gilmore, C. J. (1990). *Acta Cryst.* A**46**, 284–297.
Buseck, P. R., Cowley, J. M. & Eyring, L. (1988). *High Resolution Transmission Electron Microscopy and Associated Techniques*. Oxford University Press.
Cava, R. J., Batlogg, B., Krajewski, J. J., Rupp, L., Schneemeyer, L. F., Siegrist, T., Van Dover, R. B., Marsh, P., Peck, W. F. Jr, Gallagher, P. K., Glarum, S. H., Marshall, J. H., Farrow, R. C., Waszczak, J. V., Hull, R. & Trevor, P. (1988). *Nature (London)*, **336**, 211–214.
Cheng, T. Z., Wang, J. F., Wan, Z. H. & Sha, B. D. (1994). *J. Appl. Cryst.* **27**, 430–432.
Coene, W., Janssen, G., Op de Beeck, M. & Van Dyck, D. (1992). *Phys. Rev. Lett.* **69**, 3743–3746.
Coene, W. M. J., Thust, A., Op de Beeck, M. & Van Dyck, D. (1996). *Ultramicroscopy*, **64**, 109–135.
Debaerdemaeker, T., Tate, C. & Woolfson, M. M. (1985). *Acta Cryst.* A**41**, 286–290.
Dorset, D. L. (1995). *Structural Electron Crystallography*. New York: Plenum Press.
Dorset, D. L. & Hauptman, H. A. (1976). *Ultramicroscopy*, **1**, 195.
Fan, H. F., Xiang, S. B., Li, F. H., Pan, Q., Uyeda, N. & Fujiyoshi, Y. (1991). *Ultramicroscopy*, **36**, 361–365.
Fan, H. F., Yao, J. X., Main, P. & Woolfson, M. M. (1983). *Acta Cryst.* A**39**, 566–569.
Fan, H. F., Yao, J. X. & Qian, J. Z. (1988). *Acta Cryst.* A**44**, 688–691.
Fan, H. F., Zhong, Z. Y., Zheng, C. D. & Li, F. H. (1985). *Acta Cryst.* A**41**, 163–165.
Fu, Z. Q. & Fan, H. F. (1994). *J. Appl. Cryst.* **27**, 124–127.
Fu, Z. Q., Huang, D. X., Li, F. H., Li, J. Q., Zhao, Z. X., Cheng, T. Z. & Fan, H. F. (1994). *Ultramicroscopy*, **54**, 229–236.
Han, F. S., Fan, H. F. & Li, F. H. (1986). *Acta Cryst.* A**42**, 353–356.
Hao, Q., Liu, Y. W. & Fan, H. F. (1987). *Acta Cryst.* A**43**, 820–824.
He, W. Z., Li, F. H., Chen, H., Kawasaki, K. & Oikawa, T. (1997). *Ultramicroscopy*, **70**, 1–12.
Hovmöller, S., Sjogren, A., Farrants, G., Sundberg, M. & Marinder, B. O. (1984). *Nature (London)*, **311**, 238–241.
Hu, J. J. & Li, F. H. (1991). *Ultramicroscopy*, **35**, 339–350.
Hu, J. J., Li, F. H. & Fan, H. F. (1992). *Ultramicroscopy*, **41**, 387–397.
Hu, J. J. & Tanaka, N. (1999). *Ultramicroscopy*, **80**, 1–5.
Huang, D. X., He, W. Z. & Li, F. H. (1996). *Ultramicroscopy*, **62**, 141–148.
Huang, D. X., Liu, W., Gu, Y. X., Xiong, J. W., Fan, H. F. & Li, F. H. (1996). *Acta Cryst.* A**52**, 152–157.
Jiang, H., Li, F. H. & Mao, Z. Q. (1999). *Micron*, **30**, 417–424.
Kirkland, E. J. (1984). *Ultramicroscopy*, **15**, 151–172.
Kirkland, E. J., Siegel, B. M., Uyeda, N. & Fujiyoshi, Y. (1985). *Ultramicroscopy*, **17**, 87–104.
Li, F. H. (1994). Proc. 13th Int. Congr. on Electron Microscopy, Paris, Vol. 1, pp. 481–484.
Li, F. H. & Fan, H. F. (1979). *Acta Phys. Sin.* **28**, 276–278. (In Chinese.)
Li, F. H., Wang, D., He, W. Z. & Jiang, H. (2000). *J. Electron Microsc.* **49**, 17–24.
Liu, J., Li, F. H., Wan, Z. H., Fan, H. F., Wu, X.-J., Tamure, T. & Tanabe, K. (1998). *Mater. Trans. Jpn Inst. Met.* **39**, 920–909.
Lu, B., Li, F. H., Wan, Z. H., Fan, H. F. & Mao, Z. Q. (1997). *Ultramicroscopy*, **70**, 13–22.
Misell, D. L. (1973). *J. Phys. D*, **6**, L6-9.
One, A. & Horiuchi, S. (1994). *Jpn. J. Appl. Phys.* **33**, 1839–1846.
Rouillon, T., Provost, J., Herieu, M., Groult, D., Michel, C. & Raveau B. (1989). *Physica (Utrecht) C*, **166**, 201.
Saxton, W. O. (1986). Proc. 11th Int. Congr. on Electron Microscopy, Kyoto, Japan. Post-deadline paper, 1-4.
Schiske, P. (1968). Proc. Eur. Conf. on Electron Microscopy, Rome, Italy, pp. 145–146.
Sinkler, W. & Marks, L. D. (1999). *Ultramicroscopy*, **75**, 251–268.
Tang, D., Zandbergen, H. W., Jansen, J., Op de Beeck, M. & Van Dyck, D. (1996). *Ultramicroscopy*, **64**, 265–276.
Unwin, P. N. T. & Henderson, R. J. (1975). *Mol. Biol.* **94**, 425–440.
Uyeda, N. & Ishizuka, K. (1974). Proc. 8th Int. Congr. on Electron Microscopy, edited by J. Sanders & D. Goodchild, Vol. 1, pp. 322–323.
Vainstein, B. K. (1964). *Structure Analysis by Electron Diffraction*. Oxford: Pergamon Press.
Van Dyck, D., Lichte, H. & Van der Mast, K. D. (1996). *Ultramicroscopy*, **64**, 1–15.
Van Dyck, D. & Op de Beeck, M. (1990). Proc. 12th Int. Congress on Electron Microscopy, Seattle, USA, Vol. 1, pp. 26–27.
Van Dyck, D. & Op de Beeck, M. (1996). *Ultramicroscopy*, **64**, 99–107.
Wang, D., Li, F. H. & Zou, J. (2000). *Ultramicroscopy*, **85**, 131–139.
Wolff, P. M. de (1974). *Acta Cryst.* A**30**, 777–785.
Woolfson, M. M. & Fan, H. F. (1995). *Physical and Non-physical Methods in Solving Crystal Structure*. Cambridge University Press.
Wu, X. -J., Tamura, T., Adachi, S., Jin, C. Q., Tatsuki, T. & Yamauchi, H. (1995). *Physica (Utrecht) C*, **247**, 96–104.
Yamauchi, H., Tamura, T., Wu, X. -J., Adachi, S. & Tanaka, S. (1995). *Jpn. J. Appl. Phys.* **34**, L349-L351.
Yang, S. X. & Li, F. H. (2000). *Ultramicroscopy*, **85**, 51–59.